ROYAL SOCIETY OPEN SCIENCE

royalsocietypublishing.org/journal/rsos

Research

Cite this article: Park DK, Lee MS. 2019 Kinetic study of catalytic CO_2 hydration by metal-substituted biomimetic carbonic anhydrase model complexes. *R. Soc. open sci.* **6**: 190407. http://dx.doi.org/10.1098/rsos.190407

Received: 14 March 2019
Accepted: 1 July 2019

Subject Category:
Chemistry

Subject Areas:
environmental chemistry/biochemistry/inorganic chemistry

Keywords:
carbonic anhydrase, CO_2 hydration, biomimetic model complex, potentiometric pH titration, stopped-flow spectrophotometry

Author for correspondence:
Man Sig Lee
e-mail: lms5440@kitech.re.kr

This article has been edited by the Royal Society of Chemistry, including the commissioning, peer review process and editorial aspects up to the point of acceptance.

Electronic supplementary material is available online at https://dx.doi.org/10.6084/m9.figshare.c.4585727.

THE ROYAL SOCIETY PUBLISHING

Kinetic study of catalytic CO_2 hydration by metal-substituted biomimetic carbonic anhydrase model complexes

DongKook Park and Man Sig Lee

Green Materials and Processes Group, Korea Institute of Industrial Technology (KITECH), 55 Jongga-ro, Jung-gu, Ulsan, Republic of Korea

DKP, 0000-0002-3058-4073

The rapid rise of the CO_2 level in the atmosphere has spurred the development of CO_2 capture methods such as the use of biomimetic complexes that mimic carbonic anhydrase. In this study, model complexes with tris(2-pyridylmethyl)amine (TPA) were synthesized using various transition metals (Zn^{2+}, Cu^{2+} and Ni^{2+}) to control the intrinsic proton-donating ability. The pK_a of the water coordinated to the metal, which indicates its proton-donating ability, was determined by potentiometric pH titration and found to increase in the order $[(TPA)Cu(OH_2)]^{2+} < [(TPA)Ni(OH_2)]^{2+} < [(TPA)Zn(OH_2)]^{2+}$. The effect of pK_a on the CO_2 hydration rate was investigated by stopped-flow spectrophotometry. Because the water ligand in $[(TPA)Zn(OH_2)]^{2+}$ had the highest pK_a, it would be more difficult to deprotonate it than those coordinated to Cu^{2+} and Ni^{2+}. It was, therefore, expected that the complex would have the slowest rate for the reaction of the deprotonated water with CO_2 to form bicarbonate. However, it was confirmed that $[(TPA)Zn(OH_2)]^{2+}$ had the fastest CO_2 hydration rate because the substitution of bicarbonate with water (bicarbonate release) occurred easily.

1. Introduction

The increased use of fossil fuels in this industrial era is causing a rapid increase in CO_2 concentration in the atmosphere, which contributes to global warming [1–4]. To control CO_2 concentration, several methods, such as CO_2 capture by an amine-based absorbent or carbonic anhydrase (CA) and copolymerization with an epoxide, have been studied [5–10]. Since more than one million tons per year of CO_2 has to be

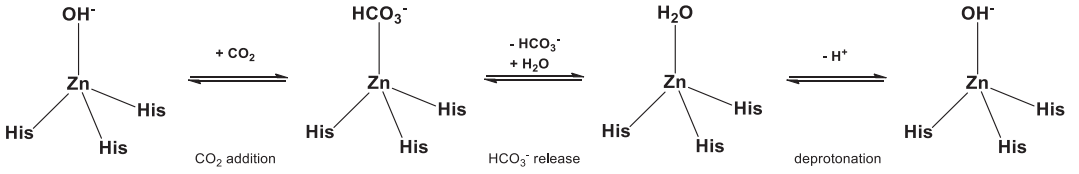

Scheme 1. Proposed mechanism for the catalytic cycle of CA.

sequestered, the importance of the development of CO_2 capture methods has been increasing. Recently, methods using CA have been of considerable interest because the enzyme hydrates and rapidly converts CO_2 to carbonic acid at a rate of at least $10^6\ M^{-1}\ s^{-1}$ [7,11,12]. However, because of the significant effects of temperature and operating pH on the catalytic activity as well as drawbacks of enzyme stability and cost, utilization of CA in an actual process is difficult [13,14]. To overcome these limitations, catalysts that mimic CA but have higher stability are currently being developed [15–18].

Most CAs have Zn^{2+} at the centre of the active site, and the metal is coordinated to one water molecule and three histidine residues. The pK_a of the water ligand is known to decrease from 15.7 to 7 owing to modulation by the Lewis acid, Zn^{2+}; thus, the hydroxide ion can be easily formed even at biological pH [19,20]. Once the nucleophilic OH^- is generated, the catalytic cycle for the formation of HCO_3^- in CA can be divided into three steps (scheme 1). The first step is CO_2 addition, in which the Zn^{2+}-bound hydroxide reacts with CO_2 to form the coordinated bicarbonate. In the second step, the bicarbonate is released by substitution with solvent water. The last step is the regeneration of the active form of CA, that is, the Zn^{2+}-bound water is deprotonated and the coordinated hydroxide is reformed ($pK_a = 7$) [21].

Deprotonation was reported to be the rate-determining step of the CA catalytic cycle [16,22,23]. This supports the hypothesis that the lower the pK_a of the water ligand, the faster the conversion rate since deprotonation would occur more easily and bicarbonate would be more rapidly produced from CO_2 [24,25]. In previous studies, the development of model catalysts has been aligned mainly with the modulation of the intrinsic proton-donating ability of the water ligand in Zn catalysts to accelerate CO_2 hydration [26]. The synthesis of model catalysts has been promoted in this direction because it was believed that the proton-donating ability can be tuned by adding an electron-withdrawing group to the ligand or stabilizing OH^- through hydrogen bonding [20,26–28]. Interestingly, the use of metal ions such as Ni^{2+} and Cu^{2+} was believed to adjust the internal pK_a of the synthesized model complex because pK_a upon hydration is lower when compared with the case of Zn^{2+}. Therefore, it would be possible to develop catalysts with a high hydration rate by using transition metals that are unlike those found in nature. In this paper, we synthesized CA model complexes containing Ni^{2+}, Cu^{2+} or Zn^{2+} coordinated to tris(2-pyridylmethyl)amine (TPA) and measured the CO_2 hydration rates by stopped-flow spectrophotometry. In addition, we determined pK_a, which represents the intrinsic proton-donating ability of the complex. Finally, we presented a detailed discussion of the reaction mechanism based on the experimental results.

2. Experimental section

2.1. General consideration

All reagents and solvents were obtained from commercial sources and used without further purification. All aqueous solutions were prepared using either deionized or distilled water. ^{1}H-NMR (500 MHz) spectra were recorded on the Varian S500 spectrometer. Elemental analyses were performed using the Thermo Scientific FlashEA 1112 elemental analyser. Mass spectra were obtained using the Agilent 6130 mass spectrometer. Fourier-transform infrared (FT-IR) spectra were recorded on the Thermo Scientific Nicolet iS50 FT-IR spectrometer. Potentiometric measurements were carried out in the pK_a mode using the Metrohm 808 Titrando titrator with the Tiamo 2.3 software and Pt1000 pH electrode. Kinetic studies were carried out in the monochromator mode using the Applied Photophysics SX20 stopped-flow spectrometer equipped with a thermoelectric temperature controller (±0.5°C).

2.2. Materials synthesis

[(TPA)Zn(OH$_2$)](ClO$_4$)$_2$ (**1**): an acetone solution (20 ml) of Zn(ClO$_4$)$_2 \cdot 6$H$_2$O (2.0 mmol, 0.74 g) was added to an acetone solution (10 ml) of TPA (2.0 mmol, 0.58 g) under nitrogen. A white precipitate was obtained upon evaporation of the solution and subsequent washing with diethylether. Yield: *ca* 60%. ^{1}H-NMR (CD$_3$OD, 500 MHz) $\delta = 8.68$ (3H, d, pyH), 8.05 (3H, t, pyH), 7.63 (3H, d, pyH), 7.60 (3H, t, pyH). MS (ESI): *m*/*z* 372 ((TPA)Zn-OH$_2$), 354 ((TPA)Zn), 471 ((TPA)Zn-OH$_2$ + ClO$_4$), anal. calcd for C$_{18}$H$_{20}$Cl$_2$N$_4$O$_9$Zn: C, 37.75; H, 3.52; N, 9.78; found: C, 37.66; H, 3.42; N, 9.79.

[(TPA)Cu(OH$_2$)](ClO$_4$)$_2$ (**2**): an acetone solution (20 ml) of Cu(ClO$_4$)$_2 \cdot 6$H$_2$O (2.0 mmol, 0.74 g) was added to an acetone solution (10 ml) of TPA (2.0 mmol, 0.58 g) under nitrogen. A blue precipitate was obtained upon evaporation of the solution and subsequent washing with diethylether. Yield: *ca* 60%. MS (ESI): *m*/*z* 371 ((TPA)Cu-OH$_2$), 353 ((TPA)Cu), 470 ((TPA)Cu-OH$_2$ + ClO$_4$), anal. calcd for C$_{18}$H$_{20}$Cl$_2$N$_4$O$_9$Cu: C, 37.87; H, 3.53; N, 9.82; found: C, 38.49; H, 3.69; N, 9.87.

[(TPA)Ni(OH$_2$)](ClO$_4$)$_2$ (**3**): an acetone solution (20 ml) of Ni(ClO$_4$)$_2 \cdot 6$H$_2$O (2.0 mmol, 0.73 g) was added to an acetone solution (10 ml) of TPA (2.0 mmol, 0.58 g) under nitrogen. A dark-blue precipitate was obtained upon evaporation of the solution and subsequent washing with diethylether. Yield: *ca* 60%. MS (ESI): *m*/*z* 366 ((TPA)Ni-OH$_2$), 465 ((TPA)Ni-OH$_2$ + ClO$_4$), 348 ((TPA)Ni).

[(TPA)Ni(OH$_2$)](SO$_4$) (**4**): Ni(SO$_4$) $\cdot 6$H$_2$O (1.0 mmol, 0.26 g) and TPA (1.0 mmol, 0.29 g) were dissolved in 10 ml of MeOH. After evaporation of the solution, the compound was crystallized in a 2 : 1 (v/v) mixture of MeOH and acetone to obtain dark-blue crystals (yield: 50%).

2.3. Single-crystal X-ray diffraction

A single crystal of **4** was mounted at room temperature on the tips of quartz fibres coated with Paratone-N oil and cooled under a stream of cold nitrogen. Intensity data were collected on the Bruker CCD area diffractometer, which runs the SMART software, with Mo Kα radiation ($\lambda = 0.71073$ Å). The structure was solved by direct methods and refined on F^2 using the SHELXTL software. Multi-scan absorption correction was applied using SADABS, which is part of the SHELXTL software. The structure was checked for higher symmetry by the PLATON program. Data collection and experimental details are summarized in the electronic supplementary material, table S1.

2.4. Potentiometric pH titration

The electrode system was calibrated with Metrohm standard buffer solutions (pH 4.00, 7.00 and 9.00) before titration. The aqueous solution of each complex (1.0 mM) was added to 2.0 mM HNO$_3$ (I = 0.1 M, NaNO$_3$), and the mixture was stirred at 25°C. Titrations were performed with a standardized 0.1 M NaOH solution, and the pH was monitored to identify the half-equivalence point using the Tiamo 2.3 software.

2.5. Kinetic measurements using a stopped-flow spectrophotometer

The CO$_2$ hydration rate was measured using methods similar to those used previously, using the stopped-flow spectrometer [16,27]. Prior to the experiments, a saturated CO$_2$ solution was prepared by spraying deionized water with 100% CO$_2$ for at least 1 h at 25°C. Using Henry's constant, the CO$_2$ concentration of this solution was calculated to be 33.8 mM. In addition, a solution containing 0.1 M *N*-(1,1-dimethyl-2-hydroxyethyl)-3-amino-2-hydroxypropanesulfonic acid (AMPSO) buffer, 0.2 M NaClO$_4$ and 5×10^{-5} M Tymol blue indicator (pH 9.0, adjusted with NaOH) was purged with N$_2$ gas for 1 h to remove dissolved CO$_2$. The saturated CO$_2$ solution and buffer solution were rapidly mixed at a 1 : 1 volume ratio in a stopped-flow spectrophotometer, and the absorbance at $\lambda = 596$ nm was recorded over time to determine the uncatalysed rate. Solutions of each catalyst (1 mM TPA-M) in AMPSO buffer solution were prepared under N$_2$ atmosphere.

The initial rate v_{int} of TPA-M was determined by rapidly mixing the saturated CO$_2$ solution and TPA-M solution and fitting the first 10% (10 s) of the time-dependent absorbance data to a single exponential decay function. The absorbance change was measured four times. v_{int} was estimated using the equation

$$v_{\text{int}} = Q(A_0 - A_e)\left[\frac{\mathrm{d}(\ln(A - A_e))}{\mathrm{d}t}\right]_{t \to 0},$$

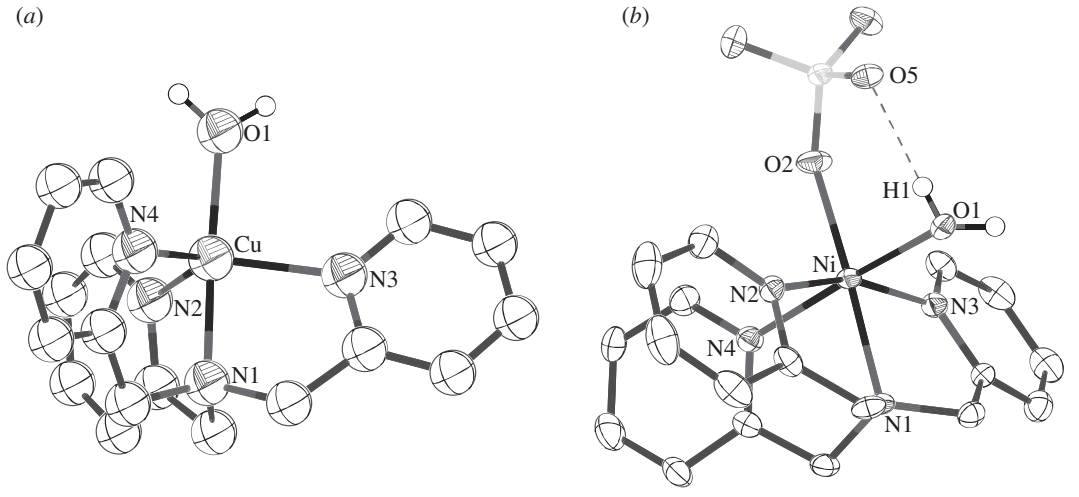

Figure 1. Crystal structures of **2** (*a*) and **4** (*b*).

where A_0 and A_e are the initial and final absorbance values. Q is the buffer factor estimated from the AMPSO buffer solution and HCl concentration using a previously described method [16]. The rate constant k_{obs} for TPA-M is the slope of the plot of $v_{init}/[CO_2]$ versus [TPA-M].

3. Results and discussion

To efficiently design the structure of a catalyst for the formation of HCO_3^- from CO_2, it is very important to understand the reaction mechanism and reaction factor of the catalytic activity. One of the most important factors in controlling the reaction rate of a CA model catalyst is the structure of the surrounding ligands, which determines the electronic state of the central metal ion [18–20,29]. Thus far, several researchers have synthesized CA model compounds that contain macrocyclic or tripodal-like N4 and N3 ligands to activate CO_2 hydration [16,20,27,30]. Although the natural CA has an N3 ligand coordination environment around the metal ion, model catalysts that have an N4 ligand are reported to show higher catalytic activity than those that have an N3 ligand [16,31]. Recently, a computational study of the DFT wave function has shown that the N4 ligand has monodentate ground state HCO_3^- binding modes with Zn, while the N3 ligand allows bidentate ground state HCO_3^- binding modes [16]. This shows that the N4 ligand has better catalytic efficiency than that of the N3 ligand because of the lower dissociation energy of HCO_3^- (HCO_3^- release step) [32]. Moreover, compared with the N3 ligand, the N4 ligand is less likely to dimerize during the formation of the metal complex. This can be beneficial in investigating the reaction mechanism and factors [20]. Finally, an N4 ligand containing pyridine shows higher water solubility compared to that of another N4 ligand containing benzimidazole, which has been widely used in the synthesis of CA model catalysts [16,27]. Therefore, we synthesized CA model catalysts with various metal ions using the pyridine-containing N4 ligand, TPA and investigated the influence of the metal ion on the activation of CO_2 hydration.

3.1. Characterization of model complexes

The structure of a model catalyst with the $[(TPA)M\text{-}OH_2]^{2+}$ motif is critical to understand the acidity of the catalyst. Currently, structures of **2** containing a copper ion have been reported [33], but not those of **1** and **3**. Although the crystal structure of **1** has been obtained, specific information is missing [34]. Various Zn^{2+} complexes containing $Zn(ClO_4)_2$, $Zn(SO_4)$ and $Zn(NO_3)_2$ were crystallized to obtain information on the structure of compound **1**; however, crystallization unfortunately yielded only thin, needle-shaped crystals. To confirm the structure of compound **3,** X-ray diffraction of compound **4**, which has SO_4^{2-} instead of ClO_4^-, was performed. The crystal structures of **2** and **4** are shown in figure 1, and the selected bond distances and bond angles are listed in table 1 [35]. The structure of **4** shows Ni hexacoordinated with TPA, water and SO_4^{2-}. The bond length of three $Ni\cdots N_{pyridine}$ bonds is narrowly distributed from 2.056 to 2.082 Å, while the bond length of the fourth $Ni\cdots N_{pyridine}$ bond is slightly longer at 2.102(3) Å. In the crystal structure of $[(TBA)Zn\text{-}OH_2]^{2+}$ [TBA = tris(2-benzimidazolylmethyl)amine], which contains benzimidazole instead of pyridine, the bond length of

Table 1. Selected bond lengths (Å) and bond angles (°).

$[(TPA)Cu(OH_2)](ClO_4)_2$ (**2**)			
Cu–O1	1.980(5)	Cu–N1	1.941(6)
Cu–N2	2.054(6)	Cu–N3	2.038(7)
Cu–N4	2.069(6)		
O1–Cu–N1	177.8(2)	O1–Cu–N2	94.5(2)
O1–Cu–N3	98.9(2)	O1–Cu–N4	99.4(2)
N1–Cu–N2	83.4(2)	N1–Cu–N3	81.7(3)
N1–Cu–N4	82.1(2)	N2–Cu–N3	119.9(2)
N2–Cu–N4	118.2(3)	N3–Cu–N4	116.8(2)
$[(TPA)Ni(OH_2)](SO_4)$ (**4**)			
Ni–O1	2.094(2)	Ni–O2	2.045(3)
H1–O5	1.97(7)	Ni–N1	2.102(3)
Ni–N2	2.082(3)	Ni–N3	2.056(3)
Ni–N4	2.076(3)		
O1–Ni–O2	92.74(13)	O1–Ni–N1	92.73(13)
O1–Ni–N2	87.84(11)	O1–Ni–N3	92.87(11)
O1–Ni–N4	171.72(12)	O1–Ni–N2	87.81(11)
O2–Ni–N1	173.57(11)	O2–Ni–N2	101.58(13)
O2–Ni–N3	95.84(14)	O2–Ni–N4	92.57(12)
N1–Ni–N2	81.99(13)	N1–Ni–N3	80.53
N1–Ni–N4	82.37(12)	N2–Ni–N3	162.52(12)
N2–Ni–N4	843.87(12)	N3–Ni–N4	92.90(12)

Table 2. Observed pK_a of complexes **1, 2** and **3**.

complexes	1	2	3
pK_a	8.0	7.6	6.0

$Zn\cdots N_{amine}$ bond is definitely long compared with that of the $Zn\cdots N_{bezimidazole}$ bond; thus, it has been claimed that TBA acts as an N3 ligand despite being an N4 ligand [27,30]. Similarly, an N4 ligand with a central tertiary amine bound to a metal ion may serve as a pseudo-N3 ligand when it is observed to have a long $M\cdots N_{amine}$ bond length [36]. The distance between the Ni ion and water molecule is the typical $Ni\cdots O$ bond length of 2.094(2) Å, and the water molecule has a strong intramolecular hydrogen bonding interaction with SO_4^{2-}.

The presence of a water molecule in complexes **1, 2** and **3** was also confirmed by studying the O–H vibration (electronic supplementary material, figure S1). At around 1610 cm^{-1}, all complexes have a sharp band that is consistent with the bending vibration of the OH group. The stretching vibration of water, typically observed at around 3300 cm^{-1}, appears at 3414 and 3232 cm^{-1} for **2** and 3232 cm^{-1} for complex **3**. Unusually, **1**, which is a Zn complex, has two vibration peaks; one at 3335 cm^{-1} and other at 3256 cm^{-1}. Compared with the O–H vibration of a free water molecule (3506 cm^{-1}), a water molecule coordinated to a metal, such as in complexes **1**, **2** and **3**, is commonly observed at low frequency [37].

In CO_2 hydration by CA, deprotonation is a very important step that determines the reaction rate. Therefore, the acidity, which is relevant to the deprotonation step of CA model catalysts **1**, **2** and **3**, is a fundamental parameter that indicates the ease of formation of nucleophilic hydroxide ion at neutral pH. The acidity of $[(TPA)M\text{-}OH_2]^{2+}$ was measured by potentiometric pH titration, and the results are shown in table 2.

Table 3. Experimentally observed rate constant k_{obs}, pH-independent rate constant k_{ind} and standard deviation (units are $M^{-1}\,s^{-1}$).

complex	k_{obs}	k_{ind}	σ_{obs}	Δk
1	645.7	710.3	14.6	64.6
2	526.4	527.0	34.8	0.6
3	542.3	563.9	4.3	21.6

The pK_a of **1** is 8.0, as previously reported [38], while those of **2** and **3** are 7.6 and 6.0, respectively. These results are consistent with previous studies showing that water ionization increases in the order $Zn < Co \ll Cu$, Ni when the metal ion in CA is substituted with different first-row transition metal ions [39–41]. This trend is probably due to the difference in the acidities of the metal ions. In particular, the pK_a of **3**, which contains Ni^{2+}, is significantly lower than those of **1** and **2**.

3.2. Kinetics of CO_2 hydration by model complexes

In CO_2 hydration by CA, deprotonation is known as the rate-determining step; thus, it is believed that for artificial catalysts that mimic the enzyme, a lower pK_a can increase the hydration rate. To understand the effect on catalytic activity when pK_a is systemically modified by changing the metal, the k_{obs} values of **1**, **2** and **3** were measured. Because CO_2 hydration is expected to be very fast, a fast kinetic measurement method, stopped-flow spectrophotometry, was used. The results are shown in table 3 and electronic supplementary material, table S2. The chemical species that is directly active in CO_2 hydration is not LM-OH_2 but the deprotonated LM-OH^-. CO_2 hydration by LM-OH_2 involves the following series of reactions:

$$\text{LM-OH}_2 \xrightarrow{k_a} \text{LM-OH}^- + \text{H}^+,$$

$$\text{LM-OH}^- + \text{CO}_2 \xrightarrow{k_{obs}} \text{LM-HCO}_3^-$$

and

$$\text{LM-HCO}_3^- + \text{H}_2\text{O} \longrightarrow \text{LM-OH}_2 + \text{HCO}_3^-.$$

The composition ratio of LM-OH_2 and LM-OH^- is determined by acid-base equilibrium; thus, k_{obs} can be represented as k_{ind} (pH-independent form) (table 3 and electronic supplementary material, figure S2).

The absorbance change ($A_0 - A_e$) that occurs during hydration was about 0.41, and the initial k_{obs}, which represents 10% of the total reaction, was obtained by fitting ($A_0 - A_e$) to a single exponential decay function. Unexpectedly, **1** has the fastest reaction rate at 645.7 $M^{-1}\,s^{-1}$.

Complex **1** has the largest difference between k_{obs} and k_{ind} ($\triangle k = 64.6\ M^{-1}\,s^{-1}$, 10.0% increase), while **2** and **3** have Δk of 21.6 (4.0% increase) and 0.6 $M^{-1}\,s^{-1}$ (0.1% increase), respectively. A large Δk indicates that the amount of LM-OH^- is less than that of LM-OH_2 at pH 9. That is, LZn-OH_2, which has the highest pK_a, has fewer LZn-OH^- species at pH 9 than those of LNi-OH_2 and LCu-OH_2. The subsequent reaction of LM-OH^- and CO_2 is an acid-base reaction, and the difference in reaction rate for this step is small. When exposed to air, a dinuclear LZn-OH^- forms the trinuclear complex $(LZn)_3CO_3$, which has a triply bridging carbonate ligand [42,43]. LCu-OH^- also rapidly forms the corresponding $(LCu)_3CO_3$ crystals [42,44]. On the other hand, LNi-OH^- forms crystals in the form of L–Ni–(μ-CO_3)–Ni–L on reaction with CO_2 [45–47]. The structure of LM-HCO_3^-, which is consistent with CO_2 addition, was reported several times with respect to CO_2 fixation. CO_2 insertion into LM-OH^- occurs very fast, and the complex is also known to be capable of easily absorbing atmospheric CO_2 [43].

Earlier in the discussion, we addressed the pK_a of various metal-TPA complexes. Many studies argue that the rate-determining step of CA is either the deprotonation of the water ligand or release of bicarbonate [16,19,22,24,25,48]. Our results from potentiometric pH titration and stopped-flow spectrophotometry suggest that bicarbonate release is the rate-determining step for LNi-OH_2 and LCu-OH_2 because these complexes have lower pK_a but slower k_{obs} than those of LZn-OH_2. LNi-OH_2 has the most frequent deprotonation, although bicarbonate release from the Ni^{2+} site does not occur easily. On the other hand, because the pK_a of LZn-OH_2 is relatively high, deprotonation of the water ligand does not occur as easily as it does in LNi-OH_2 and LCu-OH_2. However, the substitution of bicarbonate with solvent water can be inferred to occur considerably rapidly (scheme 2).

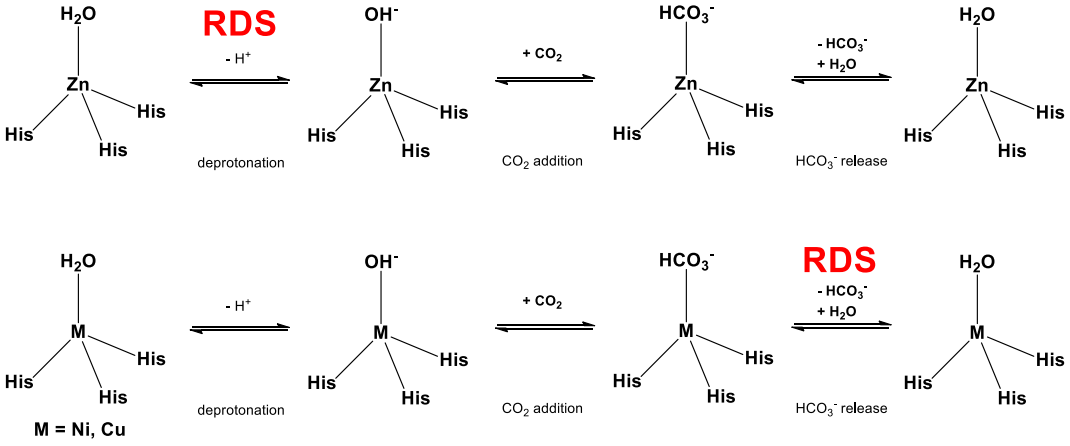

Scheme 2. Proposed catalytic cycle and rate-determining step of different model complexes.

The substitution of bicarbonate with water in CA is described by the Lindskog mechanism (oxygen transfer) [49,50]. When Zn-HCO_3^- is formed by the reaction between CO_2 and Zn-OH^-, bicarbonate is coordinated to Zn as a bidentate ligand. Hence, the Zn–O bond with hydroxide is cleaved and the carbonyl oxygen is newly coordinated to Zn, which is later substituted with water. In this mechanism, the mode of bicarbonate coordination to Zn is both unidentate and bidentate. However, in the case of Ni complex, substitution with solvent water would not occur easily because bicarbonate coordinated to Ni forms bidentate. Recently, the pK_a of Co-substituted CA was reported to be 6.6, which is lower than the pK_a of Zn-CA (6.9) [51]. However, the activity of Co-substituted CA was about three times lower than that of Zn-CA. As shown in this study, this is probably because bicarbonate release in Co-substituted CA does not occur easily.

As discussed, it is necessary to design a ligand that considers not only the active site of the natural CA but also the secondary coordination sphere in order to achieve a rate as high as that of the natural CA through the synthesis. In the case of Zn, the substitution reaction of bicarbonate and water molecules is faster than that of Cu and Ni, which suggests that mimic CA can be synthesized using Zn. However, the deprotonation reaction of Zn-bound water is slow due to high pK_a. To overcome this, it is possible to increase the acidity of Zn by additionally introducing an electron-withdrawing group such as the sulfonyl group into the ligand [27]. Moreover, the secondary coordination sphere of natural CA is controlled by various hydrogen bonds such as Thr-199, Glu-117, Asn-244 and Gln-92 to control the acidity of Zn [52,53]. Therefore, the catalytic efficiency of mimic CA will become closer to that of natural CA by designing a ligand to lower the pK_a of Zn-bound water.

4. Conclusion

We have synthesized CA model catalysts with Zn^{2+}, Ni^{2+} or Cu^{2+} using TPA, a pyridine-containing N4 ligand, and investigated the effect of the metal ion on the CO_2 hydration rate. We observed that pK_a, which shows the intrinsic proton-donating ability of each complex, increased in the order **3** < **2** < **1** because of the difference in acidities of the metal ions.

The k_{obs} for CO_2 hydration decreased in the order **1** > **3** > **2**, that is, **2**, which had relatively low pK_a had the slowest k_{obs}. This is because while the deprotonation of water was easy, the substitution of bicarbonate with water (bicarbonate release) was difficult. In other words, in terms of CO_2 conversion rate, the kinetic data for the CA model catalyst with Zn^{2+} implies that the advantage of the bicarbonate release step is greater than the water deprotonation step.

As with many previous CA model catalytic studies, if the intrinsic proton-donating ability can be increased by using Zn^{2+}, a catalyst with excellent efficiency can be developed. However, if a CA model catalyst is developed to realize various functions existing not only in the first coordination sphere (active site) of the CA but also in the secondary coordination sphere (surrounding environment), a CO_2 hydration rate close to that of natural CA can be realized.

Data accessibility. Electronic supplementary material is available at the Dryad Digital Repository: https://doi.org/10.5061/dryad.gn8723p [35]. Crystallographic data of compound **4** was deposited at the Cambridge Crystallographic Data Centre (CCDC) with deposition numbers of CCDC 1883607.

Authors' contributions. D.K.P. carried out the design of the study, participated in data analysis and wrote the manuscript. M.S.L. gave valuable suggestions on the writing of the manuscript. All the authors have approved the manuscript.
Competing interests. We declare no competing interests.
Funding. This study has been conducted with the support of the Korea Institute of Industrial Technology as 'Development of eco-friendly chemical materials and processing for casting, JA-18-0001.'
Acknowledgements. We thank the Korea Institute of Energy Research (KIER) for stopped-flow spectrophotometry measurement.

References

1. Peter SC. 2018 Reduction of CO_2 to chemicals and fuels: a solution to global warming and energy crisis. *ACS Energy Lett.* **3**, 1557–1561. (doi:10.1021/acsenergylett.8b00878)
2. Mac Dowell N, Fennell PS, Shah N, Maitland GC. 2017 The role of CO_2 capture and utilization in mitigating climate change. *Nat. Clim. Change* **7**, 243–249. (doi:10.1038/nclimate3231)
3. Cox PM, Betts RA, Jones CD, Spall SA, Totterdell IJ. 2000 Acceleration of global warming due to carbon-cycle feedbacks in a coupled climate model. *Nature* **408**, 184–187. (doi:10.1038/35041539)
4. Anwar MN, Fayyaz A, Sohail NF, Khokhar MF, Baqar M, Khan WD, Rasool K, Rehan M, Nizami AS. 2018 CO_2 capture and storage: a way forward for sustainable environment. *J. Environ. Manage.* **226**, 131–144. (doi:10.1016/j.jenvman.2018.08.009)
5. Rochelle GT. 2009 Amine scrubbing for CO_2 capture. *Science* **325**, 1652 LP–1654 LP. (doi:10.1126/science.1176731)
6. Kar S, Sen R, Goeppert A, Prakash GKS. 2018 Integrative CO_2 capture and hydrogenation to methanol with reusable catalyst and amine: toward a carbon neutral methanol economy. *J. Am. Chem. Soc.* **140**, 1580–1583. (doi:10.1021/jacs.7b12183)
7. Tan S-I, Han Y-L, Yu Y-J, Chiu C-Y, Chang Y-K, Ouyang S, Fan K-C, Lo K-H, Ng I-S. 2018 Efficient carbon dioxide sequestration by using recombinant carbonic anhydrase. *Process Biochem.* **73**, 38–46. (doi:10.1016/j.procbio.2018.08.017)
8. Bhagat C, Dudhagara P, Tank S. 2017 Trends, application and future prospectives of microbial carbonic anhydrase mediated carbonation process for CCUS. *J. Appl. Microbiol.* **124**, 316–335. (doi:10.1111/jam.13589)
9. Liu Q, Wu L, Jackstell R, Beller M. 2015 Using carbon dioxide as a building block in organic synthesis. *Nat. Commun.* **6**, 5933. (doi:10.1038/ncomms6933)
10. Darensbourg DJ, Yeung AD. 2014 A concise review of computational studies of the carbon dioxide–epoxide copolymerization reactions. *Polym. Chem.* **5**, 3949–3962. (doi:10.1039/C4PY00299G)
11. Peirce S, Perfetto R, Russo ME, Capasso C, Rossi M, Salatino P, Marzocchella A. 2017 Characterization of technical grade carbonic anhydrase as biocatalyst for CO_2 capture in potassium carbonate solutions. *Greenhouse Gases Sci. Technol.* **8**, 279–291. (doi:10.1002/ghg.1738)
12. Aggarwal M, Chua TK, Pinard MA, Szebenyi DM, McKenna R. 2015 Carbon dioxide 'trapped' in a β-carbonic anhydrase. *Biochemistry* **54**, 6631–6638. (doi:10.1021/acs.biochem.5b00987)
13. Gladis A, Gundersen MT, Neerup R, Fosbøl PL, Woodley JM, von Solms N. 2018 CO_2 mass transfer model for carbonic anhydrase-enhanced aqueous MDEA solutions. *Chem. Eng. J.* **335**, 197–208. (doi:10.1016/j.cej.2017.10.111)
14. Tran DN, Balkus KJ. 2011 Perspective of recent progress in immobilization of enzymes. *ACS Catalysis* **1**, 956–968. (doi:10.1021/cs200124a)
15. Floyd WC, Baker SE, Valdez CA, Stolaroff JK, Bearinger JP, Satcher JH, Aines RD. 2013 Evaluation of a carbonic anhydrase mimic for industrial carbon capture. *Environ. Sci. Technol.* **47**, 10 049–10 055. (doi:10.1021/es401336f)
16. Koziol L, Valdez CA, Baker SE, Lau EY, Floyd WC, Wong SE, Satcher JH, Lightstone FC, Aines RD. 2012 Toward a small molecule, biomimetic carbonic anhydrase model: theoretical and experimental investigations of a panel of zinc(II) aza-macrocyclic catalysts. *Inorg. Chem.* **51**, 6803–6812. (doi:10.1021/ic300526b)
17. Sahoo PC, Kumar M, Puri SK, Ramakumar SSV. 2018 Enzyme inspired complexes for industrial CO_2 capture: opportunities and challenges. *J. CO_2 Util.* **24**, 419–429. (doi:10.1016/j.jcou.2018.02.003)
18. Marchetti L, Levine M. 2011 Biomimetic catalysis. *ACS Catal.* **1**, 1090–1118. (doi:10.1021/cs200171u)
19. Kim JY, Kulik HJ. 2018 When is ligand pK_a a good descriptor for catalyst energetics? In search of optimal CO_2 hydration catalysts. *J. Phys. Chem. A* **122**, 4579–4590. (doi:10.1021/acs.jpca.8b03301)
20. Parkin G. 2004 Synthetic analogues relevant to the structure and function of zinc enzymes. *Chem. Rev.* **104**, 699–768. (doi:10.1021/cr0206263)
21. Lindskog S. 1997 Structure and mechanism of carbonic anhydrase. *Pharmacol. Ther.* **74**, 1–20. (doi:10.1016/S0163-7258(96)00198-2)
22. Maupin CM, McKenna R, Silverman DN, Voth GA. 2009 Elucidation of the proton transport mechanism in human carbonic anhydrase II. *J. Am. Chem. Soc.* **131**, 7598–7608. (doi:10.1021/ja8091938)
23. Silverman DN, Lindskog S. 1988 The catalytic mechanism of carbonic anhydrase: implications of a rate-limiting protolysis of water. *Acc. Chem. Res.* **21**, 30–36. (doi:10.1021/ar00145a005)
24. Duda D, Tu C, Qian M, Laipis P, Agbandje-McKenna M, Silverman DN, McKenna R. 2001 Structural and kinetic analysis of the chemical rescue of the proton transfer function of carbonic anhydrase II. *Biochemistry* **40**, 1741–1748. (doi:10.1021/bi002295z)
25. Fisher Z, Hernandez Prada JA, Tu C, Duda D, Yoshioka C, An H, Govindasamy L, Silverman DN, McKenna R. 2005 Structural and kinetic characterization of active-site histidine as a proton shuttle in catalysis by human carbonic anhydrase II. *Biochemistry* **44**, 1097–1105. (doi:10.1021/bi0480279)
26. Lesnichin SB, Shenderovich IG, Muljati T, Silverman D, Limbach H-H. 2011 Intrinsic proton-donating power of zinc-bound water in a carbonic anhydrase active site model estimated by NMR. *J. Am. Chem. Soc.* **133**, 11 331–11 338. (doi:10.1021/ja203478j)
27. Nakata K, Shimomura N, Shiina N, Izumi M, Ichikawa K, Shiro M. 2002 Kinetic study of catalytic CO_2 hydration by water-soluble model compound of carbonic anhydrase and anion inhibition effect on CO_2 hydration. *J. Inorg. Biochem.* **89**, 255–266. (doi:10.1016/S0162-0134(01)00419-6)
28. Cronin L, Foxon SP, Lusby PJ, Walton PH. 2001 Syntheses and structures of M(L)(X)BPh4 complexes {M = Co(II), Zn(II); L = cis-1,3,5-tris[3-(2-furyl)prop-2-enylideneamino]cyclohexane, X = OAc, NO3}: structural models of the active site of carbonic anhydrase. *J. Biol. Inorg. Chem.* **6**, 367–377. (doi:10.1007/s007750100211)
29. Yamauchi O, Odani A, Takani M. 2002 Metal–amino acid chemistry. Weak interactions and related functions of side chain groups. *J. Chem. Soc. Dalton Trans.* **2002**, 3411–3421. (doi:10.1039/B202385G)
30. Echizen T, Ibrahim MM, Nakata K, Izumi M, Ichikawa K, Shiro M. 2004 Nucleophilic reaction by carbonic anhydrase model zinc compound: characterization of intermediates for CO_2 hydration and phosphoester hydrolysis. *J. Inorg. Biochem.* **98**, 1347–1360. (doi:10.1016/j.jinorgbio.2004.04.022)
31. Zhang X, van Eldik R. 1995 A functional model for carbonic anhydrase: thermodynamic and kinetic study of a tetraazacyclododecane complex of zinc(II). *Inorg. Chem.* **34**, 5606–5614. (doi:10.1021/ic00126a034)
32. Rains JGD, O'Donnelly K, Oliver T, Woscholski R, Long NJ, Barter LMC. 2019 Bicarbonate inhibition of carbonic anhydrase mimics hinders catalytic efficiency: elucidating the mechanism and gaining insight toward improving speed

and efficiency. *ACS Catal.* **9**, 1353–1365. (doi:10.1021/acscatal.8b04077)

33. Nagao H, Komeda N, Mukaida M, Suzuki M, Tanaka K. 1996 Structural and electrochemical comparison of copper(II) complexes with tripodal ligands. *Inorg. Chem.* **35**, 6809–6815. (doi:10.1021/ic960303n)
34. Ito M, Fujita K, Chitose F, Takeuchi T, Yoshida K, Takita Y. 2002 General acid-promoted hydrolysis of phosphate ester in [ZnII(bnp)(tpa)](ClO4) (tpa = tris(2-pyridylmethyl)amine, bnp = bis(p-nitro-phenyl) phosphate); plausible functional model for P1 nuclease. *Chem. Lett.* **31**, 594–595. (doi:10.1246/cl.2002.594)
35. DongKook P, Man Sig L. 2019 Data from: Kinetic study of catalytic CO_2 hydration by metal-substituted biomimetic carbonic anhydrase model complexes. Dryad Digital Repository. (doi:10.5061/dryad.gn8723p)
36. Xiao Z-A, Jiang T-T. 2011 Aqua-{tris-[(1H-benzimidazol-2-yl-κN)meth-yl]amine}-zinc 5-(dimethyl-amino)-naphthalene-1-sulfonate perchlorate 2.5-hydrate. *Acta Crystallogr. E Struct. Rep. Online* **67**, m1755. (doi:10.1107/S1600536811047453)
37. Nair MS, Joseyphus RS. 2008 Synthesis and characterization of Co(II), Ni(II), Cu(II) and Zn(II) complexes of tridentate Schiff base derived from vanillin and dl-α-aminobutyric acid. *Spectrochim. Acta, Part A* **70**, 749–753. (doi:10.1016/j.saa.2007.09.006)
38. Mareque-Rivas JC, Prabaharan R, Parsons S. 2004 Quantifying the relative contribution of hydrogen bonding and hydrophobic environments, and coordinating groups, in the zinc(ii)–water acidity by synthetic modelling chemistry. *Dalton Trans.* **2004**, 1648–1655. (doi:10.1039/B402084G)
39. Han R, Parkin G. 1991 Unidentate versus bidentate coordination of nitrate ligands: relevance to carbonic anhydrase activity. *J. Am. Chem. Soc.* **113**, 9707–9708. (doi:10.1021/ja00025a065)
40. Looney A, Parkin G. 1994 Molecular structure of {.eta.3-HB(pz)3}$ZnNO_3$: comparison between theory and experiment in a model carbonic anhydrase system. *Inorg. Chem.* **33**, 1234–1237. (doi:10.1021/ic00084a045)
41. Lindskog S, Malmström BG. 1962 Metal binding and catalytic activity in bovine carbonic anhydrase. *J. Biol. Chem.* **237**, 1129–1137.
42. Bazzicalupi C *et al.* 1996 CO_2 fixation by novel copper(II) and zinc(II) macrocyclic complexes. A solution and solid state study. *Inorg. Chem.* **35**, 5540–5548. (doi:10.1021/ic9603262)
43. Murthy NN, Karlin KD. 1993 A dinuclear zinc hydroxide complex which traps atmospheric carbon dioxide: formation of a tri-zinc complex with a triply bridging carbonate group. *J. Chem. Soc. Chem. Commun.* **1993**, 1236–1238. (doi:10.1039/C39930001236)
44. Yan S, Cui J, Liu X, Cheng P, Liao D, Jiang Z, Wang G, Wang H, Yao X. 1999 Trinuclear Cu(II) and Zn(II) complexes bridged by μ_3-carbonato anion. *Sci. China Ser. B Chem.* **42**, 535–542. (doi:10.1007/BF02874277)
45. Ito M, Sakai K, Tsubomura T, Takita Y. 1999 Transesterification by (hydroxo)nickel(II) complex in the presence of external alcohol. *Bull. Chem. Soc. Jpn* **72**, 239–247. (doi:10.1246/bcsj.72.239)
46. Marsh RE, Kapon M, Hu S, Herbstein FH. 2002 Some 60 new space-group corrections. *Acta Crystallogr. B* **58**, 62–77. (doi:10.1107/S0108768101017128)
47. Ito M, Takita Y. 1996 Atmospheric CO_2 fixation by dinuclear Ni(II) complex, [TPANi(II)(μ-OH)2Ni(II)TPA](ClO4)2 (TPA = tris(pyridylmethyl)amine). *Chem. Lett.* **25**, 929–930. (doi:10.1246/cl.1996.929)
48. Zhang X, van Eldik R, Koike T, Kimura E. 1993 Kinetics and mechanism of the hydration of carbon dioxide and dehydration of bicarbonate catalyzed by a zinc (II) complex of 1,5,9-triazacyclododecane as a model for carbonic anhydrase. *Inorg. Chem.* **32**, 5749–5755. (doi:10.1021/ic00077a017)
49. Merz KM, Banci L. 1997 Binding of bicarbonate to human carbonic anhydrase II: a continuum of binding states. *J. Am. Chem. Soc.* **119**, 863–871. (doi:10.1021/ja963296a)
50. Bräuer M, Pérez-Lustres JL, Weston J, Anders E. 2002 Quantitative reactivity model for the hydration of carbon dioxide by biomimetic zinc complexes. *Inorg. Chem.* **41**, 1454–1463. (doi:10.1021/ic0010510)
51. Kogut KA, Rowlett RS. 1987 A comparison of the mechanisms of CO_2 hydration by native and Co^{2+}-substituted carbonic anhydrase II. *J. Biol. Chem.* **262**, 16 417–16 424.
52. Piazzetta P, Marino T, Russo N, Salahub DR. 2015 Direct hydrogenation of carbon dioxide by an artificial reductase obtained by substituting rhodium for zinc in the carbonic anhydrase catalytic center. A mechanistic study. *ACS Catal.* **5**, 5397–5409. (doi:10.1021/acscatal.5b00185)
53. Yu F *et al*. 2014 Protein design: toward functional metalloenzymes. *Chem. Rev.* **114**, 3495–3578. (doi:10.1021/cr400458x)